Electrochimica Acta 54 (2008) 835–843

Contents lists available at ScienceDirect

Electrochimica Acta

journal homepage: www.elsevier.com/locate/electacta

A model for the electrochemical reduction of metal oxides in molten salt electrolytes

Pritish Kar*, James W. Evans

Materials Science & Engineering Department, University of California, Berkeley, CA 94720-1760, United States

ARTICLE INFO

Article history:
Received 7 April 2008
Received in revised form 16 June 2008
Accepted 16 June 2008
Available online 28 June 2008

Keywords:
Electro-deoxidation
Titanium and alloys
Modeling
Mixed metal oxides
Molten salt

ABSTRACT

The reduction of numerous metal oxides is being investigated by electro-deoxidation in molten salts due to the low-oxygen content advantage these processes offer. One of these processes is the Fray–Farthing–Chen (FFC) process that involves the direct reduction of titanium dioxide to titanium. A model for the multi-stage reduction of titanium dioxide to titanium is reported herein. The modeling approach adopted is based on the porous electrode theory used for studying lithium-ion batteries. [J.S. Newman, C.W. Tobias, J. Electrochem. Soc. 109 (12) (1962) 1183; K.E. Thomas, J.S. Newman, T.M. Darling, in: B. Scrosati, W. van Schalkwijk (Eds.), Advances in Lithium-Ion Batteries, Kluwer Academic Publishers, New York, 2002; J.S. Newman, K.E. Thomas, Electrochemical Systems, 3rd ed., Wiley-Interscience, 2004; V. Srinivasan, J.S. Newman, J. Electrochem. Soc. 151 (10) (2004) A1517; V. Srinivasan, J.S. Newman, J. Electrochem. Soc. 151 (10) (2004) A1530; J. Christensen, V. Srinivasan, J.S. Newman, J. Electrochem. Soc. 153 (3) (2006) A560; J.S. Newman, K.E. Thomas, H. Hafezi, D.R. Wheeler, J. Power Sources 119 (SI) (2003) 838; C.R. Pals, J.S. Newman, J. Electrochem. Soc. 142 (10) (1995) A3274]. The reduction of an individual sintered pellet of TiO_2 as it undergoes electro-deoxidation in a molten salt bath of $CaCl_2$ is modeled. This model has been applied to study the effect of physical variables such as the porosity, radius of pellet, radius of grains (particle size) in the pellet and the effect of starting with a partially reduced oxide. The effect of calcium titanate formation on the reduction is also incorporated and it is shown that if the reduction is started with a pellet of partially reduced titanium dioxide, one can avoid titanate formation. Though the FFC process is not completely successful in complete reduction due to titanate formation and needs to be developed further it has succeeded in the reduction of metals that are not as complex as the titanium oxygen system. This model could also be used for studying the reduction of other metal and mixed oxides such as SiO_2, NiO, Cr_2O_3, Nb_2O_5 and ZrO_2 that are simpler to reduce than TiO_2.

1. Introduction

One of the earliest explanations of the FFC process [9–23] is the oxygen ionization mechanism shown in reaction (1). The experimental setup for the laboratory investigation of the FFC process is that shown in Fig. 1(a) and (b). In (a) the cell shows two pressed and sintered pellets of TiO_2 that are placed at the bottom of a graphite or titanium crucible which also functions as the cathodic current feeder. The two pellets in (b) are threaded onto a Kanthal wire (the current feeder) and suspended in the molten salt. The sintered pellets of TiO_2 are made the cathode in the electrolytic cell with a graphite anode. The electrolyte in the cell is molten calcium chloride that is used for its stability in the voltage range applied in the process and also offers a high-oxide ion solubility [24,25] necessary for oxygen removal from the titanium oxides:

$$TiO_2 + 2xe^- \rightarrow xO^{2-} + TiO_{2-x} \quad (1)$$

The process occurs by multiple steps as has been presented by Fray et al. [9–20] and Dring et al. [21–23] with the aid of voltammetry analysis. The results of Dring et al. have been modeled [26–27] to derive the physical parameters for each of the lower oxides. During the reduction process these TiO_2 pellets are reduced to Ti through a series of lower oxides after the Magneli phases (Ti_4O_7 and higher) in the order Ti_3O_5, Ti_2O_3 and TiO. The Ti is removed from the cell as solid pellet after the reaction is complete and is washed and dried for further metallurgical processing. Recently, it has been shown that there is formation of a number of titanates ($CaTiO_3$, $CaTi_2O_4$) [28–30] because of the availability of titanium in different oxidation states. These titantes impede the complete reduction of titanium since their reduction is not kinetically favorable under the experimental conditions. Theoretically, for the reduction of

* Corresponding author at: P.O. Box 4842, Berkeley, CA 94704-0842, United States. Tel.: +1 510 449 5095.
E-mail address: pkar2005@gmail.com (P. Kar).

0013-4686/$ – see front matter © 2008 Elsevier Ltd. All rights reserved.
doi:10.1016/j.electacta.2008.06.040

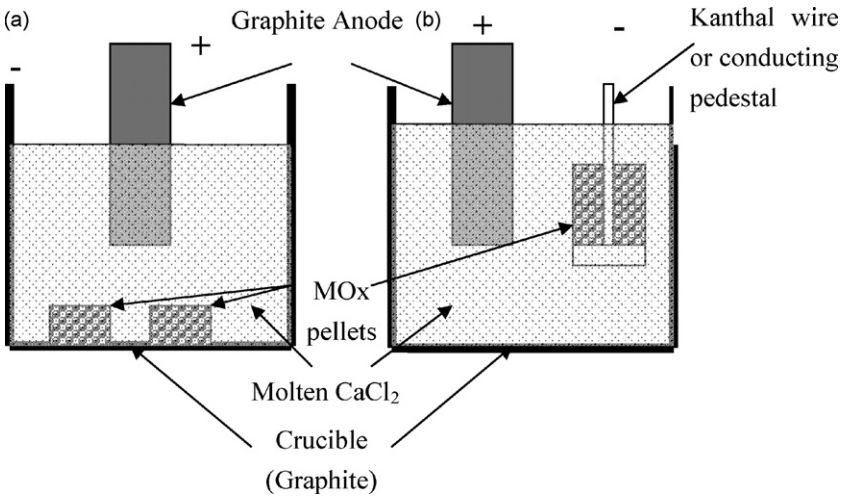

Fig. 1. Schematic diagram of two ((a) and (b)) different arrangement of the FFC process experiment [16].

titanium oxides to succeed one would need to investigate different electrolytes that have similar or better properties as molten $CaCl_2$ or explore the economic viability of using partially reduced titanium dioxide pellets. Partially reduced titanium dioxide pellets can be prepared by subjecting the pellets to reduction in hydrogen or in a plasma reactor. The FFC process has been successfully applied to the reduction of numerous other metal oxides like zirconium dioxide [31–33], chromium sesquioxide [34,35], silicon dioxide [36], terbium oxide [37], tantalum oxide [38], niobium oxide [39,40] and mixed oxides like terbium–nickel oxides [41], titanium–tungsten oxides [42] and niobium–tungsten oxides [43].

2. Model development

The mathematical model for the electro-deoxidation of the titanium dioxide is an enhancement of the published models for the intercalation/de-intercalation of lithium in porous electrodes within lithium-ion batteries [2–8]. The porous solid electrode and the electrolyte permeating it are treated as two overlapping continua [1] that implies the solid and the electrolyte phase to be present everywhere in the pellet.

The geometry of the pellet constituting the two overlapping continua is shown in Fig. 2. The interfacial area between these two continua appears in the equations but the details of pore geometry are omitted in order to have a mathematically tractable solution to the governing equations. One significant difference between the lithium-ion battery and the cell of the FFC process is that the there is typically only one solid phase in the working electrode in the former. In the latter there will be at least two phases in the electrode at any instant (e.g. Ti and Ti_3O_5 or Ti and TiO). Consequently it has been presumed that the pellet of titanium and/or oxide can be represented as an agglomerate of spherical grains and the shrinking core model has been invoked to describe the reaction in each grain.

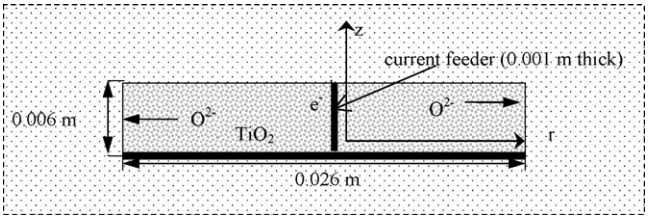

Fig. 2. Setup of the model for the modeling of electro-deoxidation of TiO_2. A doughnut-shaped pellet is wound on a current feeder of titanium shown by black lines. The pellet is the dark-shaded region of 0.026 m radius in the figure and is surrounded by electrolyte on all sides shown by the lightly shaded region.

Some of the assumptions taken into account in the modeling work are:

1. The porous solid electrode (TiO_2) and the electrolyte (molten $CaCl_2$) permeating it are treated as two overlapping continua.
2. Pellet is treated to be an assemblage of spherical grains.
3. Diffusion within pellet and grains at quasi-steady state and constant diffusion coefficients (since temperature is constant).
4. Multiple chemical reactions within grains lumped into one, as stated earlier.
5. Micro-structural variations (mostly coarsening) not taken into account.
6. Uniform potential in electrolyte surrounding pellet (hence cylindrical symmetry).

The primary physical phenomena for modeling the FFC process are:

1. Current in the electrolyte phase (molten $CaCl_2$).
2. Current in the solid phase (TiO_2).
3. Transport of the oxygen ion in the electrolyte.
4. Reaction and transport in the solid phase.

The potential in the electrolyte continuum by Thomas et al. [2] describes the current as a result of the reaction in a lithium-ion battery but for the reduction of TiO_2 by the FFC process, it is the oxygen ionization reaction similar to reaction (1). The modification results in Eq. (2):

$$i_l = -\kappa \nabla \phi_l + \frac{2\kappa RT}{F}\left[\frac{t_+^0}{\upsilon_+ z_+}\right]\nabla \ln c \qquad (2)$$

where i_l is the superficial current density in the electrolyte (A/m^2), κ is the effective ionic conductivity of the electrolyte (S/m), υ_+ is the moles of ion produced when a mole of the salt dissociates, z_+ is the charge on the calcium ion, $t_+^0 = 1 - t_-^0$, where t_-^0 is the transference number oxygen ion relative to the solvent velocity, ϕ_l is the potential in the electrolyte (V), c is the oxygen ion concentration in the electrolyte (mol/m^3), R is the universal gas constant, 8.3143 J/(mol K), T is the temperature (K), and F is the Faraday's constant, 96,484 C/equiv.

For the boundary conditions of Eq. (2), the current density in the electrolyte is set to zero at the current feeder and a potential of

1.3 V, approximating that used in typical experiments, is imposed at the pellet exterior for the boundary condition in the electrolyte continuum.

The potential in the electrode (solid) continuum follows from Ohm's law as shown in Eq. (3):

$$-\sigma\nabla\phi_s = i_s \tag{3}$$

where i_s is the superficial current density in the solid (A/m^2), ϕ_s is the potential in the solid (V), and σ is the effective electronic conductivity of the porous solid (S/m).For the boundary conditions of Eq. (3) the potential of the electrode is set to zero at the current feeder (making this the reference point for the potential differences) and the current density in the electrode is set to zero at the exterior of the pellet for the boundary condition in the electrode continuum.

The conductivities in the electrolyte (Eq. (4)) and the electrode (Eq. (5)) are calculated using the well-known Bruggeman relationship [44,45] where ε is the porosity of the pellet, κ, σ and $\kappa_{bulk}, \sigma_{bulk}$ are the effective and bulk conductivities, respectively:

$$\kappa = (\varepsilon)^{1.5}\kappa_{bulk} \tag{4}$$

$$\sigma = (1-\varepsilon)^{1.5}\sigma_{bulk} \tag{5}$$

The mass balance of oxygen ion in the electrolyte is described by Eq. (6):

$$\frac{\partial c}{\partial t} = -\nabla\cdot N_- + aj_- \tag{6}$$

where c is the oxygen ion concentration in the electrolyte, N_- is the flux of oxygen ions, j_- allows for the generation of oxygen ions at the pore surface (moles per unit pore surface per unit time), and a is the interfacial area per volume of electrode.

A steady-state assumption is made for Eq. (6) resulting in the left side being zero. The concentrated solution theory as described by Thomas et al. is used for describing the flux of the oxygen ions. An equation for the flux of oxygen ions is obtained by inverting the Stefan–Maxwell multi-component diffusion equations [3] resulting in Eq. (7):

$$N_- = -\frac{\nu_- D}{\nu RT}\frac{c_T}{c_0}\varepsilon c\nabla\mu_e + \frac{i_l t_-^0}{z_- F} + c_- v_0 \tag{7}$$

where i_l, t_-^0, R, T, F, and ε are same as explained in Eqs. (2), (4) and (5). D is the diffusion coefficient of the oxygen ions, ν is the number of moles of ions into which a mole of electrolyte dissociates, n is the number of electrons involved in the reduction reaction, υ_- is the moles of ion produced when a mole of the salt dissociates, c_0 is theconcentration of the electrolyte (mol/m^3), c_T is the total solution concentration (mol/m^3), c_- is the concentration of the oxygen ions in the electrolyte (mol/m^3), μ_e is the chemical potential of the electrolyte (J/mol), z_- is the charge of the oxygen ion, v_0 is the velocity of the ions in the electrolyte.

In Eq. (7), the first term on the right-hand side is due to the gradient in the chemical potential. The second term is due to the migration and the third term is due to convection (zero in this case). Substituting the flux equation (Eq. (7)) in the mass balance equations (Eq. (6)) results in Eq. (8) for the movement of oxygen ions in the electrolyte:

$$\nabla\cdot(\varepsilon^{1.5}D\nabla c) = -\frac{t_-^0\nabla\cdot i_l}{z_- F} \tag{8}$$

The current in the electrolyte due to the movement of the oxygen ions is described by Eq. (9):

$$i_l = -2FN_- \tag{9}$$

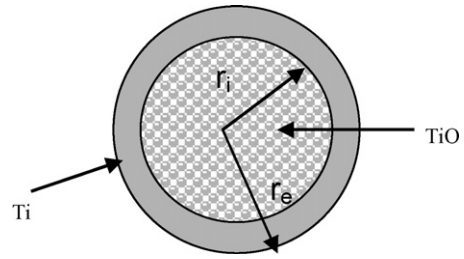

Fig. 3. A grain within the pellet showing the shrinking core and co-ordinates used.

The boundary conditions for Eq. (9) are a specified concentration (a very small value) on the exterior surface of the pellet and a zero flux at the current feeder.

For modeling the transport of oxygen in the solid phase, the quasi-steady-state shrinking core model is applied. The classical shrinking core model describes a heterogeneous reaction of a solid sphere to produce a second solid. During the reaction the sphere consists of a core of un-reacted solid (e.g. TiO_2) that is shrinking in radius as reaction proceeds. That core is surrounded by a shell of the second solid (e.g. TiO) that is thickening with time. Hence, it is a moving interface problem with the interface between the two solids moving inwards.

A feature of virtually all variants of the shrinking core model is that they have used a quasi-steady-state approximation in treating the diffusion within the shell. This is equivalent to assuming that there is negligible accumulation within the shell. This renders tractable the mathematics describing the reaction and analytical solutions (giving the radius of the core as a function of time) can usually arrived at. The shrinking core model [46–50] is used in modeling of the reaction of individual grains inside the pellets of the solid matrix. This models the reaction and transport in the solid grains making up the electrode. When applying the shrinking core model to the FFC process, the shell will be a lower oxide or titanium metal containing diffusing oxygen and the amount of oxygen in the shell might not be small compared to the amount in the core. A rigorous modeling of the reaction of a grain in a TiO_2 pellet would therefore involve a solution of the unsteady-state diffusion equation within the shell of a grain at each mesh point in the pellet. This would be a burdensome computational task compared to using the shrinking core model to describe the reaction in each grain. However, it can be shown that the quasi-steady-state solution is sufficient to describe the reaction in the FFC process [51,52].

Each grain has an outer shell (of Ti say), that surrounds a core of un-reacted material that is shrinking as reaction proceeds as shown in Fig. 3. A relationship is sought between the concentration of oxygen at the grain surface and the flux at the surface to relate this to the overall reaction in the pellet. The activity of oxygen (or concentration if an activity coefficient of 1 is assumed) at the Ti_2O_3/Ti interface or the TiO/Ti interface (when TiO was the starting material) is derived from the TiO_2-Ti phase diagram. All the reactions in the process are lumped into this reaction at the grain level.

Fig. 3 shows one grain (assumed to be spherical) and the co-ordinates used to describe the reacting grain. The shrinking core model exploits the relationship between the oxygen concentration at the grain surface, at the interface between the shrinking core–shell interface and the flux at the surface.

The equation describing the concentration of oxygen in the shell is

$$\frac{\partial c_s}{\partial t} = \frac{1}{r^2}\frac{\partial}{\partial r}\left(r^2 D_s\frac{\partial c_s}{\partial r}\right) \tag{10}$$

where c_s is the oxygen concentration in the shell in mol/m^3, D_s is the diffusion coefficient of oxygen in the shell (assumed independent of concentration) in m^2/s,and r is the radial co-ordinate within the grain in m.

It will facilitate the mathematics if a quasi-steady-state assumption is made in Eq. (10), resulting in making the left-hand side zero. It has been shown [52] that a quasi-steady-state assumption could be used for the reduction of titanium oxides.

A quasi-steady-state assumption is justified for a shrinking core model when the value of the dimensionless current density, I_d is less that 1. The dimensionless current density can be described by Eq. (11) [51]:

$$I_d = \frac{ir_e}{FD_s c_i} = \frac{I\rho r_e^2}{3FD_s c_i} \quad (11)$$

where I is the applied current per gram of particle, i is the applied current density (A/m^2), and ρ is the density of TiO_2 (kg/m^3).

For the value of the current similar to experimental values [16,28] (about 1 A in the entire pellet and for a grain it is calculated using a volumetric ratio of the grain and the pellet), I_d was calculated to be 0.000005 and hence the quasi-steady-state assumption is justified for the shrinking core model.

This pseudo-steady-state assumption reduces Eq. (10) to the following equation:

$$\frac{1}{r^2}\frac{d}{dr}\left(r^2 D_s \frac{dc_s}{dr}\right) = 0 \quad (12)$$

The quasi-steady-state Eq. (12) is applied to each individual grain with the following boundary conditions:At $r = r_i$, $c_s = c_i$ and at $r = r_e$, $c_s = c_e$where r_i is the radius of the shell–core interface within the grain (m), c_i is the oxygen concentration at the shell side of that interface (mol/m^3), r_e is the external radius of the grain (m), c_e is the oxygen concentration at the grain exterior (mol/m^3) and is a function of the potential difference between the electrode and electrolyte, respectively, resulting in $c_e = f(U)$ where $U = (\phi_s - \phi_l)$.

After integrating Eq. (12) twice and applying the boundary conditions, we get the flux at the external surface of the grains as

$$D_s \frac{dc_s}{dr} = \frac{K_1}{r_e^2} = \frac{D(c_i - c_e)}{r_e(r_i - r_e)} r_i \quad (13)$$

where K_1 is the integration constant, c_i and c_e are as explained earlier.

The flux of oxygen ions at the grain surface is then given by Eq. (14):

$$j_- = D_s \frac{c_i - c_e}{r_i - (r_i^2/r_e)} \quad (14)$$

This flux can be used in the mass balance equation in the electrolyte described in Eq. (8). From stoichiometry the shrinkage of the core within a grain is given by

$$\frac{dr_i}{dt} = -D_s \frac{(\Delta c_{interface})}{(r_i - (r_i^2/r_e))\rho_o} \quad (15)$$

where ρ_o is the oxygen concentration on the core side of the shell–core interface. An initial condition on this last equation would be $r_i = r_e$ but this condition results in an infinite initial reaction rate (diffusion in the shell cannot be rate controlling if the shell does not exist) so that r_i was set to a little less than r_e ($r_i = 0.9r_e$) initially in the program script. The implementation of Eq. (15) is updated at each step using a forward difference approach at each time step to yield the current value of r_i.

Another phenomenon occurring during the FFC process for titanium is the formation of perovskite phase of calcium titanate ($CaTiO_3$) [28–30]. The perovskite formation is a parasitic reaction for the reduction and can impede the reaction while simultaneously reducing the current density. For this purpose, we need to look at the potential-pO^{2-} (also called the Littlewood/Delarue) diagram for the titanium oxygen system constructed and described by Dring et al. [21]. This diagram shows the range of stability for the various oxides at different oxygen activities as well the possibility of calcium titanate ($CaTiO_3$) formation. From this diagram it can be shown that the potentials required to deoxygenate titanium to below 100 ppm O are more negative than that required for unit activity Ca formation. Hence, large negative voltages or a highly reducing electrolyte are required for lowering oxygen in titanium to very low levels.

Table 1
Physical parameters used for the solution of the model equations

κ_{CaCl_2} [53,54]	S/m	101.05
N		2
R	J/(mol K)	8.3145
T	K	1173
F	C/mol	96,484
ρ_{TiO_2} [55]	kg/m^3	4260
ε		0.5
R	μm	5
D_{solid} [56]	cm^2 s	4×10^{-17}
D_{CaCl_2} [57,58]	cm^2 s	2.5×10^{-9}

At a pO^{2-} value of about 5, $CaTiO_3$ would form above a potential of about −1750 mV as has been observed in experiments [21–23]. For modeling the formation of $CaTiO_3$, the location of a particular region in the pellet was examined based on the oxygen concentration in the pores and the electrode potential. It was then determined whether calcium titanate would occur depending on the location of the point in the potential-pO^{2-} diagram. The model is incapable of predicting the morphology of titanate formation, for example, the extent to which the titanate blocks the pores or the area available for any subsequent dissolution of the titanate. Consequently for those regions of the pellet where titanate formation had occurred it was assumed that no further reaction took place and the source terms in Eqs. (2), (3) and (8) were set to zero (Table 1).

A Boolean expression relating the conductivity to x in TiO_x was used in the model with the values being used from the data by Walsh et al. [59].

The above equations were implemented in a Matlab® script file within the finite element software FEMLAB™ version 3.0a (now COMSOL™) and simulations were carried out in two dimensions (the radial (x) and axial (y) co-ordinates of the cylindrical pellets).

The mesh used for the computation is shown in Fig. 4 and had 10,368 elements. Mesh refinement was carried out at the expense of computational efficiency for mesh sensitivity study until no variation in the results were obtained. The convergence criterion used was 1E−06. One of the rate limiting steps in the computational efficiency of Matlab®-based Femlab™ code was the set of post-interpolation steps. These are required to get the values of the variables involved for graphical analysis. Execution times on an AMD Athlon Dual-Process (2 GHz, 1 GB RAM) were of the order of tens of hours.

3. Results and discussion

The potential distribution on the electrolyte phase is shown in Fig. 5(a) and (b). The right-hand sides and the top of all the subfigures in Fig. 5 are the exterior of the pellet where the pellet is in contact with the bulk electrolyte. As described earlier, a potential value of 1.3 V was set in these boundaries. The lower side of the figure and the left-hand sides of the figures are regions where the pellet is in contact with the current feeder. The current is set as zero on these boundaries since all the current is carried by the elec-

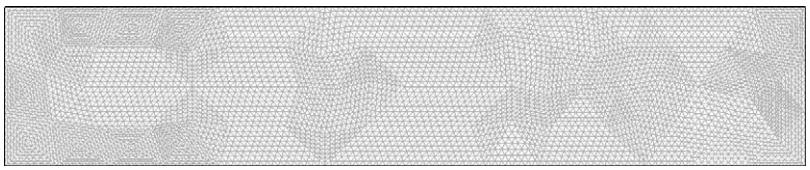

Fig. 4. The finite element mesh used for modeling the FFC process.

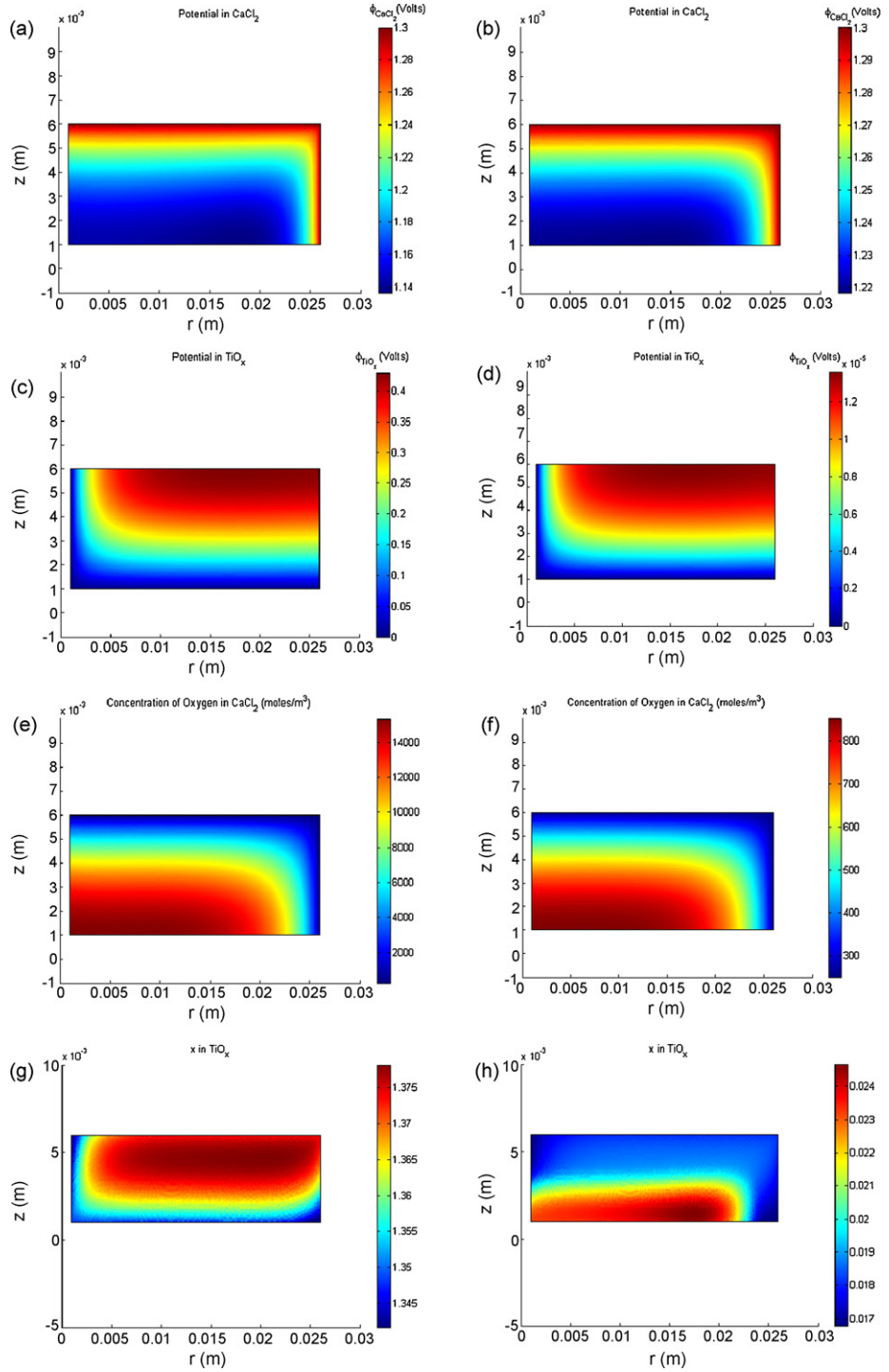

Fig. 5. Potential distribution in the electrolyte (a), solid (c) phase after 601 s (b) and after 89,701 s (d). Concentration of oxygen ions in the electrolyte phase after 601 s (e), 89,701 s (f), x in TiO_x (oxygen in the grains of titanium oxides) after 601 s (g) and 89,701 s (h).

trode in this part of the pellet. The boundary conditions are clearly satisfied since there is a potential of 1.3 V on the exterior and the gradient is zero towards the interior of the pellet.

After 10 min of reaction, there is a potential difference of 0.16 V across the electrolyte phase that has dropped to 0.08 V after 1495 min of reaction. As the pellet gets reduced the potential difference across the electrolyte drops as a consequence of a drop in current as reaction proceeds and the electrolyte gets depleted of oxygen ions. This is a direct result of increasing diffusion path lengths in the grains because of which there are lesser oxygen ions in the electrolyte phase.

Fig. 5(c) and (d) show the variation of the potential in the solid phase of the pellet at various times. The regions of the pellet in contact with the current feeder had a boundary condition of 0 V. The solid phase is not very conductive initially and hence the potential difference across the pellet is quite large. Initially this poor conductivity confines reaction to regions of the pellet with both close proximity to the current feeder and ready access to the pellet exterior that facilitates oxygen ion transport out of the pores. The potential in the solid is directly related to the amount of reduction and can be explained by taking into account the profiles of oxygen in the solid phase with progression of the reduction. The potential differences becomes negligible with increasing reduction as shown by Fig. 5(d) indicating reaction less non-uniform throughout the pellet as will be explained later on.

The concentration of oxygen in the electrolyte within the pores is initially high because the overall rate of reaction is initially high. Therefore a higher gradient of oxygen ion concentration is needed to drive the diffusion of oxygen ions out of the pores as seen in Fig. 5(e) and (f). However the rate diminishes with time and therefore so does the oxygen ion concentration (and hence the gradient) as shown in Fig. 5(e) and (f) at various reaction times. The zero flux boundary condition near the current feeder and a fixed low-oxygen ion content boundary condition at the pellet in contact with the bulk electrolyte is satisfied.

As the pellet gets reduced, TiO_2 is converted, first into lower oxides and then into Ti. In other words x in TiO_x diminishes from 2 to 0. The experimental current versus time plots for the reduction of TiO_2 is shown in Fig. 6. There is an initially increased current at the start of the reaction implying that reduction is occurring by electrochemical reaction occurring during this stage of reduction.

This reason for the very fast initial reduction along with experimental data has been given by Schwandt et al. in [28]. A summary of the reasoning provided by Schwandt et al. [28] is provided below. The similarity or the differences in the crystal structures shown below could account for the rate of the reduction reactions.

Schwandt et al. [28] show that the similarity in the crystal structures from TiO_2 to Ti_3O_5 as shown in Table 2 reduces the free energy barrier for the transformation (less reconstructive) and hence the change is fast. The formation of the Magneli phases could occur very fast kinetically because of the similarity of the crystal structures of the phases to the rutile structure and they also have similar free energies of formation [60]. On the other hand, from Table 2, TiO has a NaCl type face-centered cubic structure with high number of vacancy sites that imposes a kinetic limitation, apart from the

Table 2
Crystal structures of different titanium oxides [28]

Oxide	Crystal structure
TiO_2	Hexagonal close packed
Ti_nO_{2n-1}, $4 \le n \le 10$	Shear from hexagonal close packed
Ti_3O_5, Ti_2O_3	Hexagonal corundum
TiO	NaCl type face-centered cubic (with a number of vacancy sites)

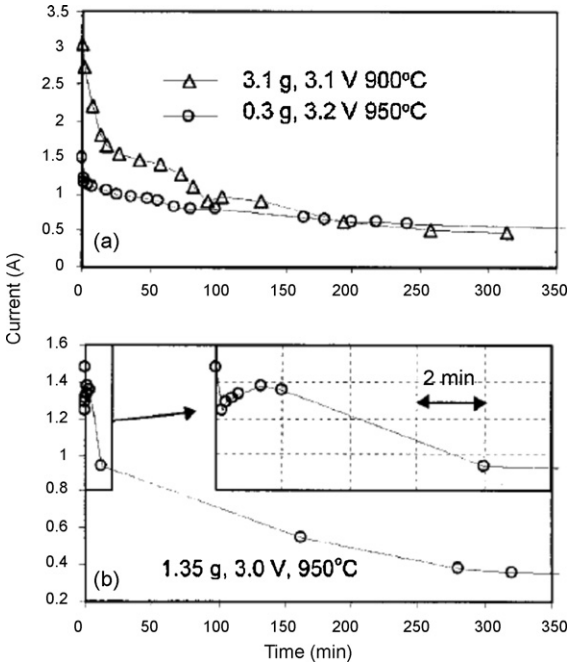

Fig. 6. Experimental data for the change in current during the reduction of pellet of TiO_2 from Fray et al.'s work [16]. In both (a) and (b), the initial high current is due to the fast reduction that subsequently becomes slow [16].

transport limitation created by the shell of Ti. As shown in Fig. 5(g) and (h), the reduction is initially fastest in the regions of the pellet with good access to both the current feeder and the exterior that facilitates the supply of electrons and the faster removal of oxygen ions, respectively. Later, when the electrode has become significantly more conductive, the proximity to the current feeder becomes inconsequential and reduction takes place preferentially near the whole external surface.

There are relatively weak horizontal potential gradients in the solid phase indicating currents that are mostly downward, rather than radially inward. There is a slight radially outward flow of current, near the pellet exterior as shown by the potential distribution in Fig. 5(c) and (d). As the pellet loses oxygen it becomes more conductive and the potential differences becomes negligible and shown by Fig. 5(c) and (d) in succeeding order of increasing time of reaction. With increasing reduction, the conductivity situation changes and the reduction scenario reverses with more reduction on the exterior that has more access to the electrolyte than the interior. This is exacerbated at the lower outer surfaces of the pellet or the upper surface near the current feeder which have access to current as well as electrolyte compared to the rest of the pellet as shown in Fig. 5(h).

An experimental plot of the reduction of the pellet with time is shown in Fig. 6 [16]. As observed initially, the curve starts out at a high current initially due to the initial electrochemical reaction and flattens out after a few hours. The curve flattens out a little towards the end of the reduction because the remaining oxygen has to diffuse through a much larger distance and the driving forces for its diffusion have diminished.

The experimental times observed [16,28] are similar to those observed with the simulations as shown in Fig. 7. A similar reasoning of large diffusion distance of oxygen ions for describing the experimental data can be used for explaining the slowly declining simulated curve. Though the axes in the two cases (current in the case of the experimental data and rate of change of x in TiO_x or rate

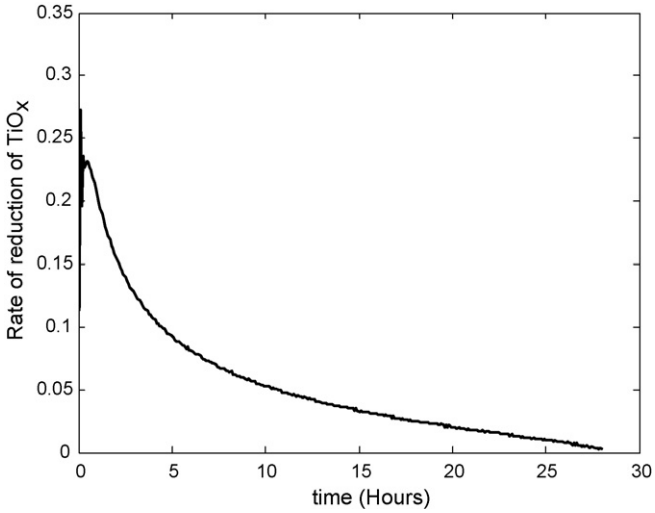

Fig. 7. Rate of reduction of TiO_x vs. time of reduction that shows that it takes about 28 h for complete reduction of the solid.

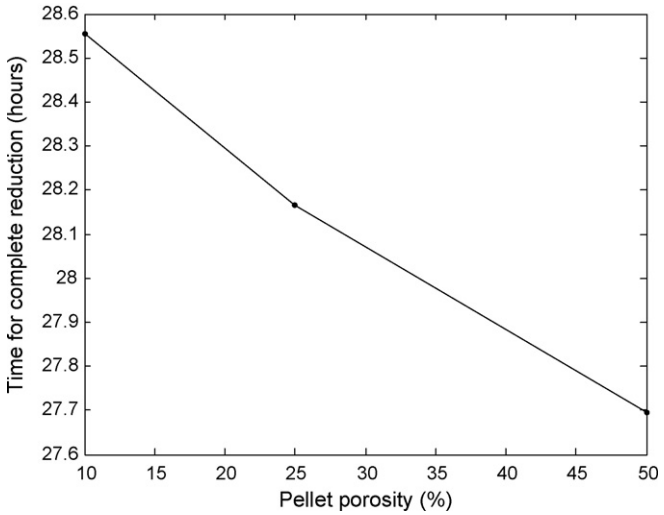

Fig. 9. The average x in TiO_x (oxygen in the grains of titanium oxides) vs. time of reduction (h) with the reaction starting with.

of change of oxygen in the lower oxides of titanium) are different, they describe the same physical phenomena of the rate of removal of oxygen from the oxides.

Some interesting parameters for experimental studies and optimization are the pellet thickness (or the height of the pellet), the average particle size within the sintered pellets, the porosity of the pellets, effect of partially reduced starting material and the effect of calcium titanate formation as has been observed in certain experiments by Fray et al. [16].

3.1. Effect of pellet thickness

The time for complete reaction with different pellet thickness is shown in Fig. 8. The time for complete reaction increases from 27 to 39 h with an increase in the pellet thickness from 1 to 15 mm. The larger diffusion distance for the oxygen ions within the thicker pellet results in a longer time of reduction. However the time for reaction shows a moderate dependence on pellet thickness reflecting the fact that the diffusion of oxygen within the grains is the dominating factor resisting to the progress of reaction. In experimental studies of Nb_2O_5 reduction [60] by the FFC process, it has been found that thicker pellets reduced for similar amounts of time contain higher oxygen than their thinner counterparts. In an industrial scale application, one has to reach a compromise between thinner pellets and tonnage limitations to make it a feasible process and needs to be calculated with respect to specific costs and comparison to the Kroll process to make it a profitable process.

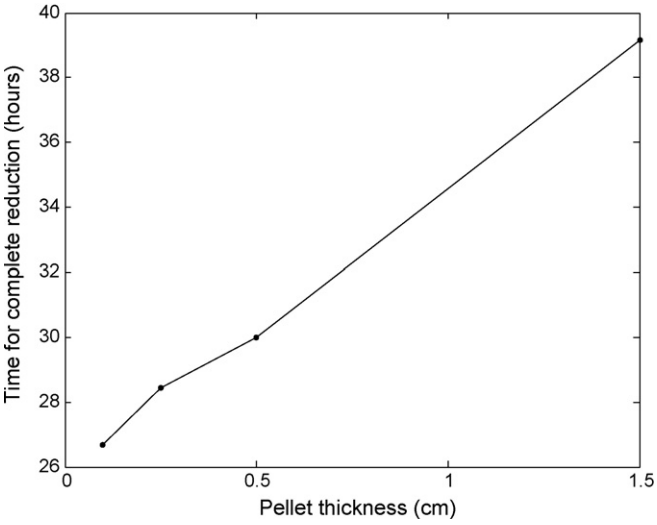

Fig. 8. The time for complete reduction (h) vs. pellet thickness (cm) shows an almost linear increase in reduction time with thickness.

3.2. Effect of porosity

The porosity of the pellets could be very important parameter for the reduction experiments. It is related to the compaction load and the temperature of the sintering process. A combination of these can cause different porosity and impact the completion times for reduction and the current consumed. However, the effect of the porosity of the pellet on the time for complete reduction shown in Fig. 9 is quite small. The completion time decreases from 28.55 to 27.7 h with the increasing porosity from 10 to 50%. This again reflects the dominance of diffusion within the grains as determining the rate of reaction. Increased porosity facilitates diffusion within the electrolyte permeating the pores but this is a lesser resistance to the progress of reaction than one within the grain.

3.3. Effect of particle (grain) radius

The particle radius is a critical parameter that can greatly influence the experimental reduction process. The effect of the particle size on the time for complete reduction is shown in Fig. 10. The time for complete reduction increases from 28 to 38.5 h with increase in the average particle radius from 5 to 15 μm. Again the importance of diffusion within the grains making up the pellet is revealed. It has been experimentally shown [40] that there is a complex relationship among the particle size and size distribution of the starting Nb_2O_5 powders, the microstructure of the sintered pellets of Nb_2O_5 and the morphology and oxygen contents of the reduced pellets. The completion time is nearly same for an increase in particle radius from 5 to 7.5 μm while there is steep increase with an increase in the radius to 15 μm. From sintering theory, it has been observed that the lower the sizes of the particles the lower the porosity since

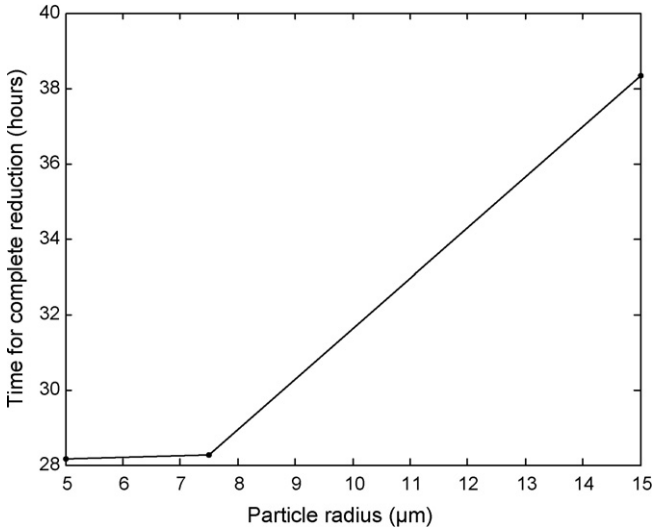

Fig. 10. The time for complete reduction (h) vs. particle radius (μm) shows an increase in reduction time with increase particle radius.

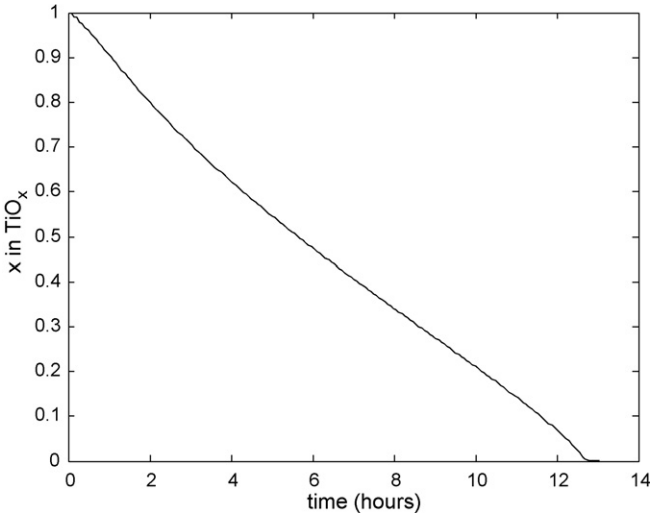

Fig. 12. The average x in TiO_x (oxygen in the grains of titanium oxides) vs. of reduction (h) with the reaction starting with TiO.

the particles tend to become very close packed. From the simulated results, a particle size of about 8 μm is the best from the point of view of a lower reduction time.

3.4. Effect of perovskite ($CaTiO_3$) formation

As described in Section 2, it is incapable of predicting the morphology of titanate formation, for example, the extent to which the titanate blocks the pores or the area available for any subsequent dissolution of the titanate. Consequently for those regions of the pellet where titanate formation had occurred it was assumed that no further reaction took place and the source terms in Eqs. (2), (3) and (8) were set to zero. The effect of titanate formation on the reduction profile with time is shown in Fig. 11. An average x in TiO_x of about 0.19 is obtained for a reduction time of about 28 h when there is titanate formation in the pellet and is a significant impediment for the complete reduction of the pellets. It has been hypothesized that titanate formation occurs from Ti_3O_5 and Ti_2O_3 that can be avoided by pellets that have been reduced partially with hydrogen prior to subjecting to electro-deoxidation.

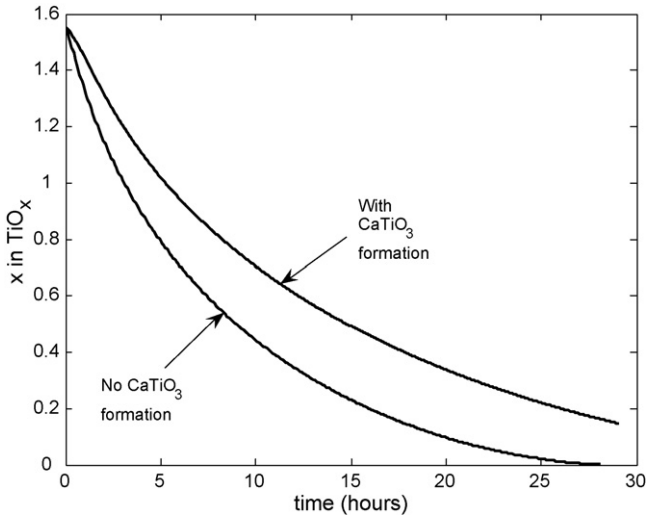

Fig. 11. The average x in TiO_x (oxygen in the grains of titanium oxides) vs. time of reduction (h).

3.5. Oxygen effect on reduction

One way of avoiding $CaTiO_3$ formation and reducing the reduction time is to start with TiO as the starting material instead of TiO_2. The effect of a starting material of TiO instead of TiO_2 is shown in Fig. 12. Apart from the difference in times taken for the reduction of the pellet, the profile of the average x in TiO_x with reduction time is almost linear. This reduction occurs considerably faster since it is started with a highly conductive pellet. Some earlier studies on reduction of titanium dioxide explored the idea of hydrogen reduction but it proved unsuccessful because of incomplete reduction beyond TiO or the difficulty in subsequent deoxidation. This would be a good experimental approach to prevent titanate formation in an industrial process with the pellets from hydrogen reduction being dropped into a molten salt bath of $CaCl_2$ for deoxidation.

4. Conclusions

A model has been developed and implemented for the reduction of titanium dioxide in molten $CaCl_2$ in the FFC process. The model makes some significant approximations, the major being that the change of microstructure with reduction can been neglected. The parametric studies carried out upon validation of the model yields parameters that would result in optimum reduction time and high productivity on the industrial application of this model. The model yields other interesting results and shows that the formation of perovskite phases (which has been hypothesized to be impeding the reaction based on experimental data) occurs under certain conditions in the pellet, which might be unavoidable using the present electrolyte and pellet compositions. One way of avoiding titanate formation is by starting with a partially reduced pellet of TiO, rather than with pellet of TiO_2.

The model can also be further refined and additional phenomena like the change in the microstructure due to the reduction could be incorporated. As developed, this model can be used in a reactor scale model to help in the industrial application and scale-up of on an FFC process based reactor for production of various metals and alloys.

References

[1] J.S. Newman, C.W. Tobias, J. Electrochem. Soc. 109 (12) (1962) 1183.

[2] K.E. Thomas, J.S. Newman, T.M. Darling, in: B. Scrosati, W. van Schalkwijk (Eds.), Advances in Lithium-Ion Batteries, Kluwer Academic Publishers, New York, 2002.
[3] J.S. Newman, K.E. Thomas, Electrochemical Systems, 3rd ed., Wiley-Interscience, 2004.
[4] V. Srinivasan, J.S. Newman, J. Electrochem. Soc. 151 (10) (2004) A1517.
[5] V. Srinivasan, J.S. Newman, J. Electrochem. Soc. 151 (10) (2004) A1530.
[6] J. Christensen, V. Srinivasan, J.S. Newman, J. Electrochem. Soc. 153 (3) (2006) A560.
[7] J.S. Newman, K.E. Thomas, H. Hafezi, D.R. Wheeler, J. Power Sources 119 (SI) (2003) 838.
[8] C.R. Pals, J.S. Newman, J. Electrochem. Soc. 142 (10) (1995) A3274.
[9] D.J. Fray, Metall. Mater. Trans. B 31 B (2000) 1153.
[10] G.Z. Chen, D.J. Fray, T.W. Farthing, Nat. Mater. 407 (5) (2000) 361.
[11] D.J. Fray, G.Z. Chen, Proceedings of the 4th International Conference on Materials Engineering for Resources, Akita, Japan, 2001, 1:1.
[12] D.J. Fray, T.W. Farthing, G.Z. Chen, Removal of oxygen from metal oxides and solid solutions by electrolysis in a fused salt, World Patent 99/64638 (1999).
[13] G.Z. Chen, D.J. Fray, T.W. Farthing, Metall. Mater. Trans. B 32 B (2001) 1041.
[14] G.Z. Chen, D.J. Fray, J. Electrochem. Soc. 149 (11) (2002) E455.
[15] G.Z. Chen, D.J. Fray, in: A.T. Tabereaux (Ed.), Light Metals, 2004.
[16] D.J. Fray, G.Z. Chen, Mater. Sci. Technol. 20 (2004) 295.
[17] A.J. Fenn, G. Cooley, D.J. Fray, L. Smith, Adv. Mater. Proc. 162 (2004) 51.
[18] D.J. Fray, G.Z. Chen, T.W. Farthing, Metal and alloy powders and powder fabrication, World Patent 02/40725 (2002).
[19] G.Z. Chen, D.J. Fray, Can. Metall. Q 41 (4) (2002) 433.
[20] G.Z. Chen, D.J. Fray, in: J.L. Anjier (Ed.), Light Metals, 2001, p. 1147.
[21] K. Dring, R. Dashwood, D. Inman, J. Electrochem. Soc. 152 (3) (2005) E104.
[22] K. Dring, R. Dashwood, D. Inman, J. Electrochem. Soc. 152 (10) (2005) D184.
[23] K. Dring, M. Jackson, R. Dashwood, H. Flower, D. Inman, Proceedings of the cost-affordable titanium symposium TMS (2004) 95.
[24] G.S. Perry, L.G. Macdonald, J. Nucl. Mater. 130 (1985) 234.
[25] D.A. Wenz, I. Johnson, R.D. Wolson, J. Chem. Eng. Data 15 (2) (1969) 252.
[26] P. Kar, J.W. Evans, Electrochem. Commun. 8 (2006) 1397.
[27] P. Kar, J.W. Evans, ECS Trans. 2 (13) (2007) 23.
[28] C. Schwandt, D.J. Fray, Electrochim. Acta 51 (2005) 66.
[29] M. Ma, D. Wang, W. Wang, X. Hu, X. Jin, G.Z. Chen, J. Alloys Compd. 420 (2006) 37.
[30] K. Jiang, H. Xiaohong, M. Ma, D. Wang, G. Qiu, X. Jin, G.Z. Chen, Angew. Chem. Int. Ed. 45 (3) (2006) 428.
[31] Q.Y. Li, J.H. Du, Z.P. Xi, Rare Met. Mater. Eng. 36 (Spl. Suppl. 3) (2007) 390.
[32] Q.Y. Li, J.H. Du, Z.P. Xi, Trans. Nonferrous Met. Soc. China 17 (Spl. Iss. A-1) (2007) S560.
[33] A.M. Abdelkader, A. Daher, R.A. Abdelkareem, Metall. Mater. Trans. B 38 (1) (2007) 35.
[34] C. Schwandt, Fray DJ, Z. Naturforsch. A: Phys. Sci. 62 (10–11) (2007) 655.
[35] G.Z. Chen, E. Gordo, D.J. Fray, Metall. Mater. Trans. B 35 (2) (2004) 223.
[36] K. Yasuda, T. Nohira, R. Hagiwara, J. Electrochem. Soc. 154 (7) (2007) E95.
[37] D.H. Wang, G.H. Qiu, Jin XB, Angew. Chem. Int. Ed. 45 (15) (2006) 2384.
[38] X.F. Hu, Q. Xu, Acta Metall. Sin. 42 (3) (2006) 285.
[39] X.Y. Yan, D.J. Fray, J. Mater. Res. 8 (2) (2003) 346.
[40] X.Y. Yan, D.J. Fray, J. Electrochem. Soc. 152 (1) (2004) D12.
[41] G.H. Qiu, D.H. Wang, X.B. Jin, Electrochim. Acta 51 (26) (2006) 5785.
[42] K. Dring, R. Bhagat, M. Jackson, J. Alloys Compd. 419 (1–2) (2006) 103.
[43] X.Y. Yan, Fray DJ, Adv. Funct. Mater. 15 (11) (2005) 1757.
[44] D.A.G. Bruggeman, Ann. Phys. 24 (1935) 636.
[45] J.C. Maxwell, A Treatise on Electricity and Magnetism, 3rd ed., Clarendon, Oxford, 1904, p. 435.
[46] M. Pritzker, Sep. Purif. Technol. 42 (2005) 15.
[47] G. Zhang, O. Ostrovski, Metall. Mater. Trans. B 32B (2007) 465.
[48] N. Lindman, D. Simonsson, Chem. Eng. Sci. 34 (1979) 34.
[49] G.F. Carey, P. Murray, Chem. Eng. Sci. 44 (4) (1989) 979.
[50] P. Carabin, D. Berk, Chem. Eng. Sci. 47 (9–11) (1992) 2499.
[51] V.R. Subramanian, H.J. Ploehn, R.E. White, J. Electrochem. Soc. 147 (8) (2000) 2868.
[52] P. Kar, J.W. Evans, Electrochim. Acta 53 (2008) 5260.
[53] A.S. Dworkin, M.A. Bredig, H.A. Bronstein, Discuss Faraday Soc. 32 (1961) 188.
[54] P.D. Ferro, B. Mishra, W. Averill, in: E.L. Roy (Ed.), Light Metals, 1991, p. 1197.
[55] E.B. Millard, Electric Conductivity: Solid and Liquid Salts, International Critical Tables:149.
[56] http://www.azom.com/details.asp?ArticleID=1179.
[57] A.N. Bagshaw, B.G. Hyde, J. Phys. Chem. Solid 37 (1976) 835.
[58] P.D. Ferro, B. Mishra, D.L. Olson, W.A. Averill, Waste Manage. 17 (7) (1997) 451.
[59] J.R. Smith, F.C. Walsh, J. Appl. Electrochem. 28 (1998) 1021.
[60] D.C. Lynch, D.E. Bullard, Metall. Mater. Trans. B 28 (1997) 447.